Surface morphology of electrospun PLA fibers : mechanisms of pore formation

Natarajan, Lakshmi; New, Jackie; Dasari, Aravind; Yu, Suzhu; Manan, Munirah Abdul

2014

Natarajan, L., New, J., Dasari, A., Yu, S., & Manan, M. A. (2014). Surface morphology of electrospun PLA fibers : mechanisms of pore formation. RSC advances, 4(83), 44082-44088.

https://hdl.handle.net/10356/101870

https://doi.org/10.1039/C4RA06215A

RSC Advances

Dynamic Article Links ►

Cite this: DOI: 10.1039/c0xx00000x

www.rsc.org/advances

Paper

Surface Morphology of Electrospun PLA fibers: Mechanisms of pore formation

Lakshmi Natarajan,[a] New Jackie,[a] Aravind Dasari,[*a] Yu Suzhu,[b] and Munirah Abdul Manan[b]

[a] *School of Materials science and Engineering (Blk N4.1), Nanyang Technological University, 50 Nanyang Avenue, Singapore 639798*
[b] *Singapore Institute of Manufacturing Technology, 71 Nanyang Drive, Singapore 638075*
[*] *Corresponding author: e-mail aravind@ntu.edu.sg, Fax +65-67909081*

Received (in XXX, XXX) Xth XXXXXXXXX 20XX, Accepted Xth XXXXXXXXX 20XX
DOI: 10.1039/b000000x

The article elucidates the mechanisms of formation of varying degrees of surface pores/pits on polylactic acid (PLA) fibers during electrospinning. The role of a combination of different parameters in governing pore formation was demonstrated. They include solvent vapor pressure (p_v), solvent miscibility/interaction with water, solubility parameter, and relative humidity (RH) within the spinning unit. Our results indicated that traditional mechanisms like thermally induced phase separation (TIPS) and vapor induced phase separation (VIPS) were not responsible in the generation of surface porosity/pits. Instead, higher RH (water vapor, a non-solvent of the polymer), and its miscibility/interaction with solvent(s) were concluded to be relatively more important than the simple presence of a high p_v solvent or a combination of high p_v and low p_v solvent systems. Further, content of high p_v solvent in the solution determined the spherical or elliptical nature of pores/pits by affecting the level of saturation of the nearby region of the interface between jet and air during the electrospinning process.

Introduction

For many biological and chemical applications involving adsorption and desorption of various organic/inorganic species on a solid, surface morphology of the latter plays an important role. To this extent, significant experimental and theoretical efforts were diverted towards understanding the effects of surface features like roughness, pores and functionalization on sorption/desorption.[1-5] Rechendorff et al.[5] showed that fibrinogen protein adsorption on evaporated tantalum films was influenced by nano-scale surface roughness. The uptake increased by almost 70% when the root-mean squared roughness increased from 2.0 to 32.9 nm. For many filtration applications and oil spill clean-up processes, the approach of surface functionalization is commonly used to allow for superior selectivity of hydrophobic hydrocarbons.[6] In addition, for faster adsorption kinetics, porous surfaces are developed with remarkable enhancements in surface area, which provide additional binding or adsorption sites.[7] The sorption mechanisms, in general, include pore-filling, hydrogen bonding interactions and hydrophobic interactions. In some cases, π–π bonding interaction and exchange of carboxyl/hydroxyl functional groups were also ascribed as sorption mechanisms.[8]

Recently, electrospinning technique, which enables production of fibers with high surface-to-volume ratios, has seen application in different fields where sorption is a critical parameter. Some of these fields include tissue engineering/drug delivery, sensors, oil adsorption, catalytic systems, and protective clothing. There are many excellent reviews on electrospinning discussing the underlying physics, interaction of surface tension of solvents and electrical forces, solution properties, etc.[9-13] Readers are encouraged to refer to those publications for an insight into fundamentals of electrospinning. Another major advantage of electrospinning is the ability to induce porosity on the fibers *in situ* during spinning, which provide additional sites for adsorption. But there are many differences (and questions) on the proposed mechanisms of pore formation in the literature. Some of the commonly reported mechanisms are TIPS, VIPS, and evaporation induced phase separation (due to difference in vapor pressure of solvents).[14-18]

TIPS is based on the phenomenon that the solvent quality usually decreases when the temperature is decreased. Conventionally, after demixing is induced, the solvent is removed by extraction, evaporation or freeze-drying.[14] In electrospinning, fibers could be directly spun into a cryogenic liquid, and as a result of sudden drop in temperature, TIPS occurs between the solvent-rich and solvent-poor regions. Subsequently, after the solvent is evaporated in a controlled manner, pores form throughout the fiber (not just on the surface). However, this method generally yields bigger pores and thicker broken fibers due to immediate freezing, which affects fiber whipping and elongation.[16] VIPS is based on precipitation by absorption/penetration of a non-solvent like water from the vapor phase into fiber jet.[17] Bognitzki et al.[19]

Cite this: DOI: 10.1039/c0xx00000x

www.rsc.org/advances

Paper

Table 1 Vapor pressure (kPa),[20] dielectric constant[20] and Hansen solubility parameters[21](MPa)$^{1/2}$ of solvents used.

Solvent	Vapor pressure (kPa)	Dielectric constant	Hansen solubility parameter (MPa)$^{1/2}$			
			δ_d	δ_p	δ_h	δ_t
Dichloromethane	58.1	8.93	18	12.3	7.2	22.9
N,N-Dimethylformamide	0.49	36.71	17.4	13.7	11.3	24.8
Methanol	16.937	32.66	15.1	12.3	22.3	29.7
1,4-Dioxane	4.95	2.209	19	1.8	7.4	20.5
1,2-Dichloroethane	11.11	10.37	19	7.4	4.09	20.8

even showed that porous fibers could be obtained by selective dissolution of electrospun polymer blends. They verified this by electrospinning polylactic acid (PLA)/polyvinylpyrrolidone (PVP) with dichloromethane (DCM) as solvent. Subsequently, porosity was obtained by either annealing the fibers to remove PLA or using water as a solvent to remove PVP.

Further, some have reported that porous fibers could be obtained during electrospinning by using a single (highly volatile) solvent through thermodynamically driven events.[16,19] In here, it was believed that the solvent-rich regions were transformed into pores. Due to fast evaporation of the solvent, phase boundaries were crossed resulting in rapid phase separation and structure formation. However, it was noted that these phase morphologies exist only on the surface of fibers, which is debatable. In another investigation, the importance of solvent volatility in inducing pores on fibers rather than phase separation was emphasized.[17] This was established by using tetrahydrofuran, THF (p_v ~21.6 kPa at 25 ^oC and boiling point, T_b ~66 ^oC), dimethylformamide, DMF (p_v ~2.7 kPa at 25 ^oC and T_b ~153 ^oC) and their combination (THF/DMF - 75/25% and 50/50%) as solvents for PS. With 100% THF, high density of pores was observed on PS fibers and they disappeared as the volatility of the mixed solvent system decreased (that is, with increase in DMF content).

Nonetheless, there are many questions on pore formation during electrospinning and it is not so direct to conclude based on only one particular factor like solvent volatility. In fact, in many studies, humidity (at which the fibers are spun) and solvent miscibility with (condensed) water are not considered (or mentioned). We believe that these in combination with vapor pressure of solvent and solubility parameter differences between solvent(s) and polymer might govern pore formation. This forms the fundamental basis of this study, that is, to elucidate the mechanisms of pore formation on fibers during electrospinning. For this purpose, PLA is chosen as the matrix and various solvents with different properties are chosen strategically (see Tables 1 and 2).

Experimental

Materials

A high molecular weight PLA, 'PLA Polymer 2003D', derived from annually renewable resources was purchased as pellets from Nature works® LLC, UK. It has a specific gravity of 1240 kg/m^3 and a glass transition temperature of 57 ºC. DCM and 1, 4 dioxane were purchased from Merck, Singapore; methanol from Fisher Scientific, UK; DMF from Tedia, US; and 1, 2-dichloroethane from Sigma Aldrich, USA. All solvents were of analytical grade (>99% purity) and used as received. Their vapor pressures, dielectric constants and Hansen solubility parameters are listed in Table 1.

Methods

Electrospinning:

A laboratory scale electrospinning unit, Nanospinner NE 300 (Innovenso Ltd., Turkey) with a bottom-up setup was used. Humidity inside the electrospinning unit was varied by using Olee UV air dehumidifier (OL-608) and monitored using a digital humidity indicator. Various solvent systems (see Table 2) and humidity levels (ranging from 25-90%) were employed. 8 wt. % PLA solutions were prepared by dissolving the required amount of PLA pellets in the solvent systems while continuously stirring (using a magnetic stirrer) for 24 hours at room temperature. The solutions were spun at a feed rate of 0.9 ml/hour and a voltage of 15-19 kV, while maintaining the distance between nozzle and collector at 120 mm.

Characterization:

Morphology of electrospun fibers was observed using a field emission scanning electron microscope (SEM) - JEOL 6340 F. Fibers were sputter coated with gold before examination at an accelerating voltage of 5-10 kV. From SEM micrographs, average fiber diameter was measured by considering around 200 fibers using Image J software. Porosity and total pore area were measured using mercury intrusion porosimeter, Micromeritics AutoPore IV 9520. The amount of material needed for porosimetry test, m±10%, is calculated using the formula,

$$m = 0.206\ \rho_B\ [(100/\%P)-1] \quad (1)$$

where, ρ_B = skeletal density of material in g/cc (without pores), %P = approximate open porosity as volume %, and m = approximate mass of material in g.

The fibers were dried overnight in vacuum oven at 45 ºC before analysis to ensure the sample is completely dry. The sample was placed in the cup of a powder penetrometer (stem volume 0.412 ml) and tested first at low pressure (6.8927 x 10^2 – 6.8927 x 10^4

Cite this: DOI: 10.1039/c0xx00000x

www.rsc.org/advances

Paper

Table 2 Electrospinning of PLA (8 wt. %) with different solvent systems (in volume %) and the end result on porosity after electrospinning at ~75% RH

Electrospinning solution combinations		Designation	Porosity at ~75% RH
Single solvent system	PLA + DCM	A1	Pores
Binary and ternary solvent system	PLA + (70%DCM + 30%DMF)	A2	No Pores
	PLA + (40%DCM + 40%DCE + 20%DMF)	A3	Pores
	PLA + (90%DCM + 10%DMF)	A4	Pores
	PLA + (90%DCM + 10%Methanol)	A5	No Pores
	PLA + (70%DCM + 30% 1,4-Dioxane)	A6	Pores

Pa) and then at high pressures ($6.8927 \times 10^2 - 6.8927 \times 10^7$ Pa) at a mercury filling pressure of 3.5824×10^3 Pa and equilibration time of 10 seconds. In this technique, mercury (non-wetting liquid) is forced into the spun fibers to assess pore volume. As the pressure is gradually increased, mercury is forced into the smaller pores. The pore radius and pressure are related by the Washburn equation (assuming that pores are cylindrical),

$$r = -2\gamma\cos\theta/p \quad (2)$$

where, θ = contact angle of mercury with the sample (130°), γ = surface tension of mercury (0.485 N/m), r = pore radius, and p = applied pressure (Pa). The volume of pores at the corresponding sizes are measured based on the volume of intrusion of mercury into the sample and thus the total pore area can be determined.

Results and discussion

Influence of solvent properties on pore formation

Single solvent system: Before discussing the electrospinning results of PLA with different combinations of solvents, it is important to identify if the mixed solvents form azeotropes or heteroazeotropes, which then demands the calculation and understanding of mixed solvent properties (like boiling point, vapor pressure, etc.). However, this is not the case here in the ratios added (see Table 2).[22] But to have a quick comparison across the systems, simple Raoult's law was used to calculate the total vapor pressure of each solvent combination. Obviously, the single solvent system of DCM has the highest p_v of ~58.1 kPa, whereas 40% DCM + 40% DCE (1,2 -dichloroethane) + 20% DMF mixture yielded the lowest ~30.3 kPa, and the rest of the systems are in-between ~43-52 kPa. But these differences could not be translated into porosity/pits on the electrospun fibers.

An SEM micrograph of PLA fibers spun at a RH of ~75% using a single solvent system (PLA/DCM) is shown in Figure 1a that reveals high density of porosity. Although the temperature in the spinning unit is constant, high p_v of DCM results in rapid solvent evaporation followed by evaporative cooling of the charged jet as it travels to the collector. This could result in TIPS. Obviously, evaporative cooling will be more effective on the surface of the fibers compared to the bulk and might as well explain the fact that these fibers only shows surface porosity and not throughout the cross-section (see Figure 1b). Apart from condensation, moisture in the ambient could also act as a non-solvent by absorption and penetrating into polymer solution during electrospinning process, as explained earlier, and result in VIPS. For this mechanism, the difference in the p_v of solvent (used in the electrospinning process) and non-solvent (from the ambient) is important as it determines which one will saturate the nearby region of the interface between jet and air. In the present case of DCM (pv ~58.1 kPa) and water (pv ~2.3 kPa), with reasonable confidence it is assumed that DCM will saturate the nearby region of the jet-air interface. This suggests that VIPS may not be the mechanism in this case. Another important parameter is the diffusion coefficient of the non-solvent in the selected polymer. This will govern the penetration efficiency and in turn determines whether pores are formed only on the surface or throughout the cross-section of the fiber.

Nonetheless, the spherical nature of the surface pores suggests that TIPS and VIPS are not the operating mechanisms (where elliptical or elongated pores along the fiber axis are more common). This means that the porosity is induced after fibers are deposited on the collector as a result of condensation of moisture in the air (as water is a non-solvent for PLA). Subsequently, these water droplets leave their imprint in the form of pores or pits on the surface of fibers (see scheme 1). This is similar to the concept of 'breath figures', which was originally introduced by Aitken[23] to explain the formation of water droplets on clean glass surfaces when exhaled breath condenses on those surfaces. Later, this was extended to describe condensation on different types of surfaces; for example, see[24,25]. Even analytical solutions that describe the evolution in time were proposed.[26] In many cases, breath figures were also used to characterize the degree of contamination on a (homogeneous) surface.[27] If the surface is contaminated, the

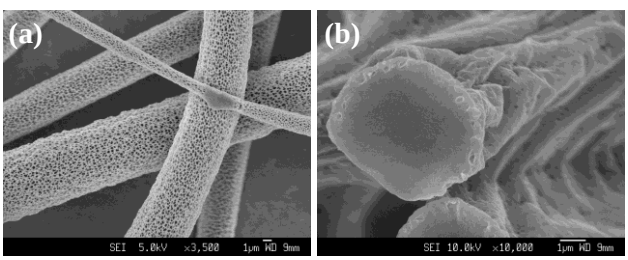

Fig. 1 SEM micrographs of PLA fibers spun at ~75% RH with 100% by volume of DCM (a) top view; and (b) cross-section.

Cite this: DOI: 10.1039/c0xx00000x

www.rsc.org/advances

Paper

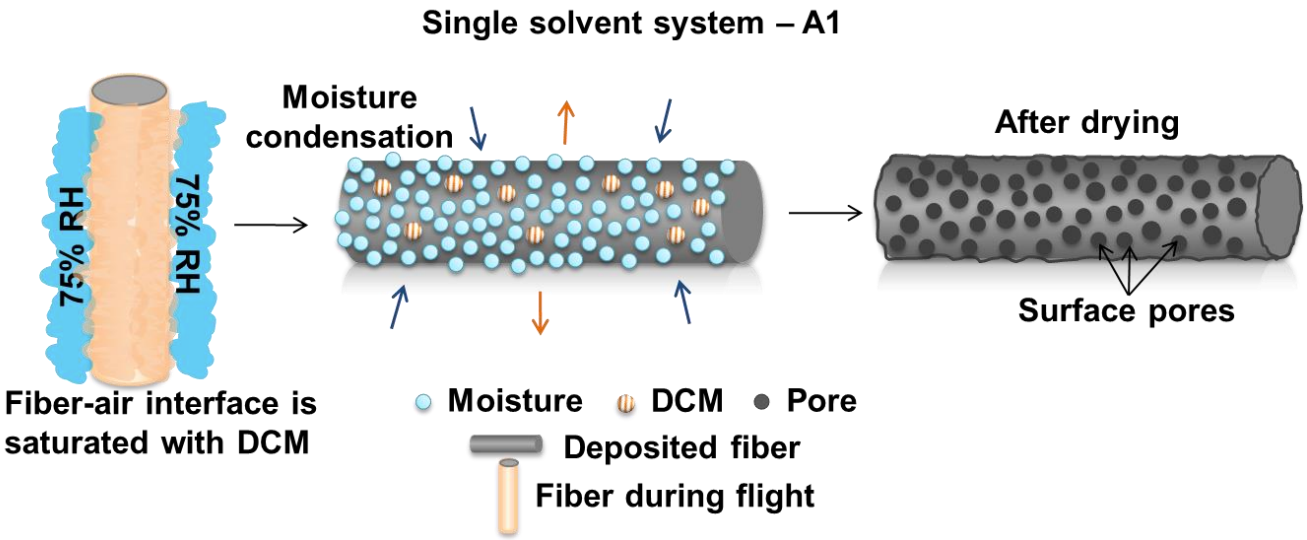

Scheme 1 Mechanism of pore formation in a single solvent system (A1).

condensation was expected to be strong leading to film formation.[24] Needless to say that %RH plays a critical role in this process.

Binary and ternary solvent systems: As discussed before in earlier studies, higher p_v solvent systems (either single or a combination) and/or higher RH levels should induce porosity. Also, porosity should decrease (and gradually disappear) as the volatility of the mixed solvent system decreases. However, this is not the case here. A2 (containing 70% of high p_v solvent, DCM) showed no pores or pits on the fibers, Figure 2a. In contrast, A3 (containing 60% of low p_v solvents, DCE and DMF), showed surface pores, Figure 2b. These differences clearly illustrate that p_v/solvent volatility is not the sole reason in inducing porous morphology on the electrospun fibers.

To explain this, it is important to understand other properties of these solvents like their miscibility and interactions with water. In A2, the solvent system was DCM/DMF in the ratio 70 to 30 by volume. Since the p_v of DCM is very high compared to DMF, it is expected to evaporate relatively quickly during the electrospinning process leaving behind DMF. Therefore, at high RH levels, after the moisture in the air condenses onto the fiber surface, the H-bond interaction of DMF with water, C−H···O, plays an important role in hindering the deposition of condensate as separate droplets. Instead it is presumed that the condensate is coalesced and spread across the fiber surface. Subsequently, after the evaporation of water, a smooth surface morphology is generated without any pores or pits. This in fact is supported by the result that if the DMF content is reduced to 10% by volume, pit/pores were observed, however at a reduced density compared to system A1 (Figure 2c).

To further elucidate on the effect of solvent miscibility/interaction with water, methanol and 1, 4-dioxane are

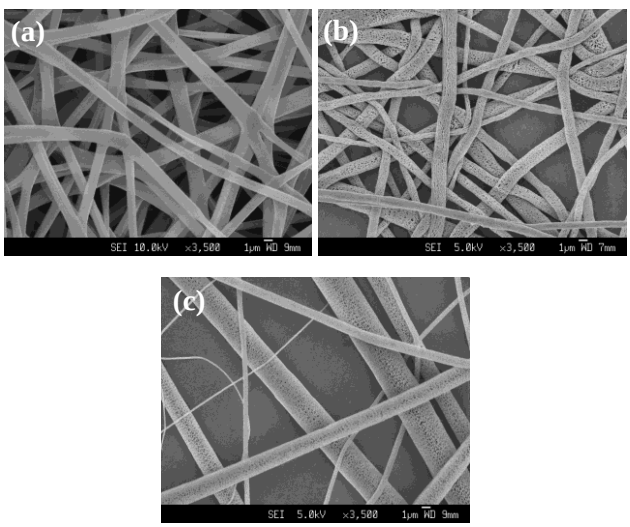

Fig. 2 SEM micrographs of PLA fibers spun at ~75% RH with different solvent combinations: (a) 70/30 DCM/DMF; (b) 40/40/20 DCM/DCE/DMF; and (c) 90/10 DCM/DMF

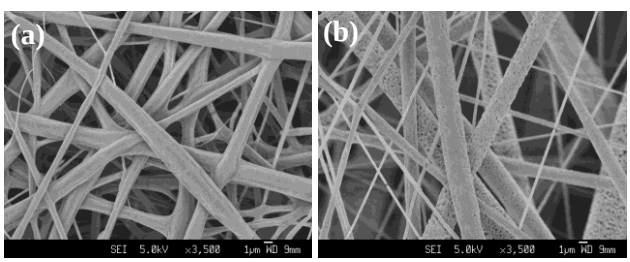

Fig. 3 SEM micrographs of PLA fibers spun at ~75% RH with different solvent combinations: (a) 90/10 DCM/methanol; and (b) 70/30 DCM/dioxane.

Cite this: DOI: 10.1039/c0xx00000x

www.rsc.org/advances

Paper

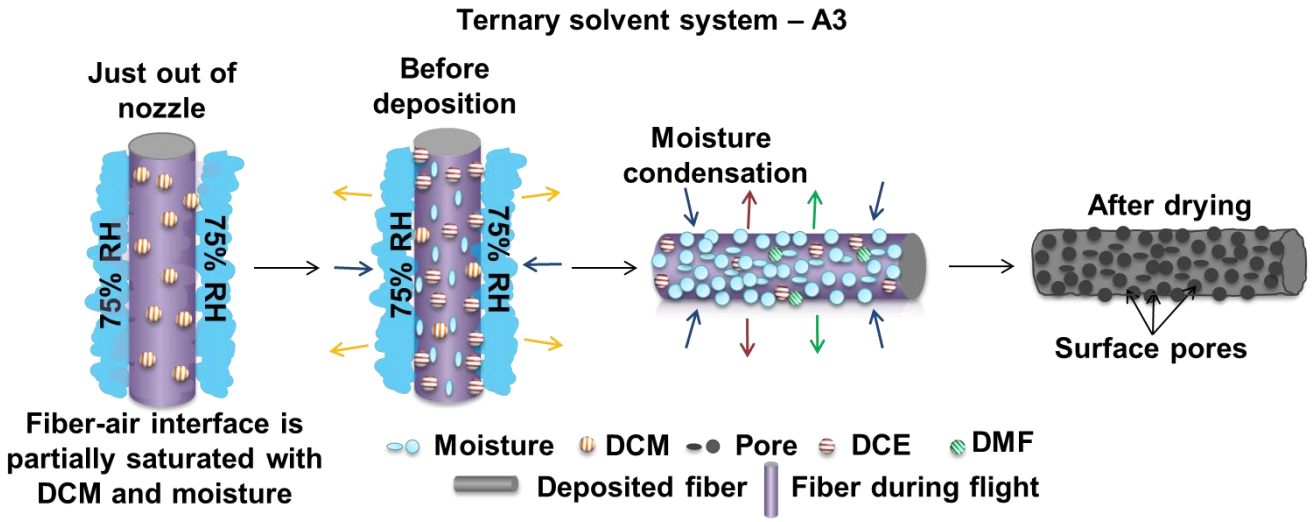

Scheme 2 Mechanism of pore formation in a ternary solvent system (A3).

chosen in combination with DCM. Both methanol and dioxane are miscible with water but their hydrogen bonding component and p_vs are different (Table 1). Although methanol's p_v is much higher than that of DMF, methanol has H-bonding component twice as that of DMF, thus enabling even a lower amount of methanol to bond with moisture/droplets. This explains why there are no pores on the surface of fibers even with 90/10 DCM/methanol (Figure 3a, A5); while 90/10 DCM/DMF showed reduced density of surface pits (Figure 2c, A4) as explained before. Also, from the SEM micrograph of A5, it is evident that the fibers are flat and more like ribbons than tubular. This indicates the slower evaporation of solvent in combination with water, thus collapsing the fibers.[28]

On the contrary, even with 30% dioxane (A6), the morphology is similar to 90/10 DCM/DMF with surface pores/pits. But 70/30 DCM/DMF didn't yield porous morphology, Figure 2a. This is despite dioxane having a similar p_v as DMF. This again reiterates the effect of solvent interaction with water.

From the above results, it is evident that at high RH levels, in the presence of low p_v solvents, their interaction with water plays a dominant role in inducing surface pores/pits. This further explains why there are pores on the fibers of A3. The solvents in A3 have huge differences in p_vs and their miscibility/interaction with water is different. DCM (p_v ~58.1 kPa) and DMF (~0.49 kPa) were discussed earlier, whereas DCE with a p_v of ~11.1 kPa is immiscible with water. Also, the density of pores at these high RH conditions is determined by the magnitude of these interactions as well as the amount of low p_v solvent. But interestingly, many of the pores are elongated along the fiber axis, giving an average aspect ratio of ~2.3. As the amount of high p_v DCM is only 40% by volume, expectedly, it cannot saturate the nearby region of the jet-air interface. This provides a chance for the water vapor in the ambient to be attracted to the positive charges distributed on the surface of fiber and condense as small droplets, thus undergoing stretching along with the fiber. This process is shown in Scheme 2.

Effect of humidity on pore formation

RH is another important factor that could influence the pore formation on the surface of fibers. Previously, it was noted that when PS with a molecular weight of 190,000 g/mol was electrospun with THF as solvent, average surface pore size increased from ~85 nm to 135 nm as the RH increased from 30% to 70%.[29] The pore size further increased to 350 nm at 70% RH when a high molecular weight (560,900 g/mol) PS was used. Change in viscosity was thought to be a possible reason for this. In contrast, Lu and Xia[15] showed that when PS (molecular weight of 300,000 g/mol) was electrospun with DMF, a hierarchical structure was formed (each fiber contained bundles of entangled fibrils) only in the RH range of 40-70%. But when the solvent was changed to THF (higher p_v of 21.6 kPa compared to DMF's 0.49 kPa), surface pores were formed at RH levels of 22%, 42%, and 62% and no pores were generated at a low RH of 2%. Nonetheless, in the present work, to understand the effect of RH, A1 and A2 systems were chosen because of their surface morphological differences and electrospinning was carried out at RH levels ranging from 25% to 75%. As expected, at relatively low RH levels (~25%), both A1 and A2 did not show any porous surface morphology (and therefore, SEM micrographs are not shown here). However, A1 showed pores at 35% RH and above; and the level of porosity increased with RH. An example of this behavior is shown in Figures 4a (RH ~35%), 4b (RH ~45%) and 1a (RH ~75%). Also, in A1, the fibers are fairly uniform in diameter at low RH due to lesser dissipation of charges during

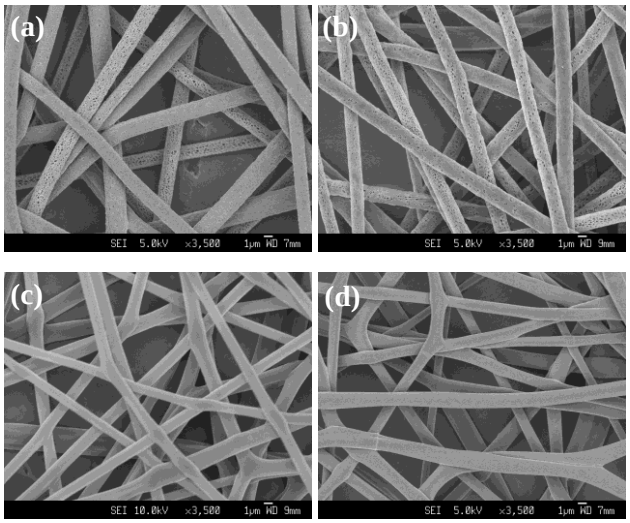

Fig. 4 SEM micrographs of A1 (a and b) and A2 (c and d) systems electrospun at different relative humidity levels (a, c – 35% and b, d – 45%).

spinning. This is quite reasonable because DCM has a low dielectric constant and a high p_v, which can cause production of inconsistent fibers if charges are dissipated easily. A2 did not show pores at all levels of humidity pointing to the effect of miscibility/interaction of DMF with water. Examples of this behavior are shown in Figures 4c and 4d.

Total pore area on the fibers

As discussed earlier, the objective of making porous fibers is to influence adsorption kinetics by enhancing surface area, and thereby providing additional binding or adsorption sites. To understand how much extra surface area was obtained by inducing porosity on the surface of fibers (and accompanied surface morphological changes like roughness), mercury intrusion porosimeter was utilized. It is well known that thermodynamically, gas/vapor condensation-evaporation and mercury intrusion-extrusion into and out of pores are similar processes. But the only difference is that they happen in opposite directions.

A2 and A3 systems were considered for porosity measurements because both these systems showed similar fiber diameters, 1.00± 0.20 μm and 1.08 ± 0.27 μm, respectively. By having this commonality and minimizing the differences in density of deposition, differences in inter-fiber porosity could be controlled. This enables an easy comparison of the effect of pores present on the surface. In A2 and A3, the area corresponding to inter-fiber porosity is 8.1 m^2/g and 8.2 m^2/g, respectively (based on Figure 5). This value is comparable to that of previous work by Yang et al.[30] in which they reported the area of inter-fiber porosity to be ~8 m^2/g for PLA fibers of similar size. By relating the average pore size as observed in SEM images with the porosimeter curve, it is clear that the peak in A3 (which is absent in A2) corresponds to the pores present on the surface. The calculated total pore area was ~31.2 m^2/g, corresponding to an average pore size of ~63.0 nm. The total area (39.3 m^2/g) is also comparable to that of 37.1 m^2/g for porous polyacrylonitrile fibers obtained by Nayani et al.[31] However, in that study, the area corresponds to core-shell fibers having a hollow core and porous sheath. The porosity was

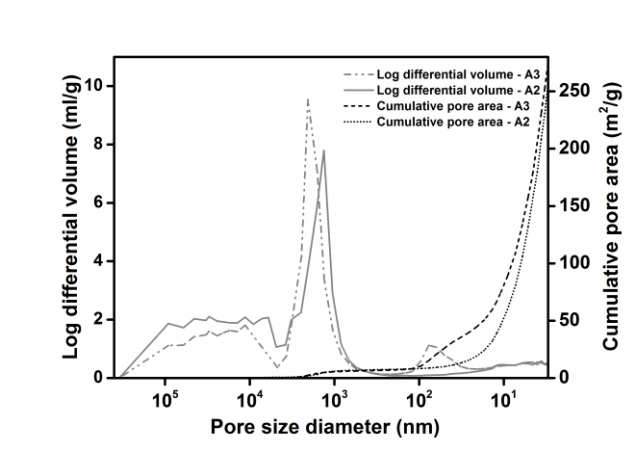

Fig. 5 Pore size diameter versus intrusion volume and cumulative pore area for A2 and A3.

obtained by non-solvent induced phase separation mechanism by directly spinning the fibers into a bath of non-solvent. In another recent study, Touny at al.[32] synthesized porous PLA fibers using reactive electrospinning where water was liberated as a by-product during the formation of monetite (which was formed *in situ* by a reaction between calcium hydroxide and orthophosphoric acid). As a result of this water-induced pore formation mechanism, as expected, pores are elongated and present throughout the fiber. But even here, the surface area of porous fibers was found to be 26.5 m^2/g at a monetite content of 28 wt. %.

In summary, this study underlines the importance of understanding various intrinsic and extrinsic parameters on pore formation during electrospinning. The obtained pore size, shape and density are independent of the fiber diameter. This was also confirmed by changing the collector distance. However, further work is required to quantify the extent of (a) moisture condensation as a result of evaporative cooling when different solvents are used; and (b) hydrogen bonding and its relation to spreading of water droplets on the fiber surface.

Nonetheless, as different applications require different levels of porosity, carefully choosing the solvent system and controlling the ambient conditions could help meet the requirements in a single step. This simplistic approach in enhancing the adsorption behavior will provide a comprehensive platform for a broad variety of applications including active food packaging, oil adsorption, moisture and odor management in fabrics, etc.

Conclusions

PLA in single, binary and ternary solvent systems with different properties were studied to understand the mechanisms of pore formation. The approaches discussed provided a simple way to fabricate fibers with different levels of porosity (surface features). The presence of spherical pores on fibers suggested that pores were formed by condensation of moisture after fiber deposition (due to evaporative cooling of fiber surface) similar to the concept of breath figures. This suggested the importance of solvent vapor pressure, relative humidity and saturation of fiber jet-air interface by a high vapor pressure solvent in inducing (spherical) pores.

In the presence of low vapor pressure solvents and at high RH

levels, solvent miscibility/interaction with water played a dominant role in inducing pores. This was demonstrated by considering binary and ternary solvent systems in which one of the solvents was miscible with water and had different hydrogen bonding parameter.

RH played a determining role in pore formation mechanisms. But at relatively low humidity levels of less than ~30%, no pores were observed on the fibers in all systems.

The total pore area of fibers (A3) was ~39.3 m^2/g, as measured by mercury porosimeter.

Acknowledgements

AD acknowledges the Academic Research Fund Tier-1 (RG45/11) from the Singapore's Ministry of Education and the Start-up-Grant from Nanyang Technological University for financially supporting parts of this research.

References

(1) Beheshtian, J.; Baei, M. T.; Peyghan, A. A. *Surf. Sci.* **2012**, *606*, 981.
(2) Bhandarkar, M.; Shelekhin, A. B.; Dixon, A. G.; Ma, Y. H. *J. Membr. Sci.* **1992**, *75*, 221.
(3) Huang, Y. W.; Gupta, V. K. *Macromolecules* **2001**, *34*, 3757.
(4) Kruk, M.; Jaroniec, M. *Chem. Mat.* **2001**, *13*, 3169.
(5) Rechendorff, K.; Hovgaard, M. B.; Foss, M.; Zhdanov, V. P.; Besenbacher, F. *Langmuir* **2006**, *22*, 10885.
(6) Akhavan, B.; Jarvis, K.; Majewski, P. *ACS Appl. Mater. Interfaces* **2013**, *5*, 8563.
(7) Gui, X. C.; Li, H. B.; Wang, K. L.; Wei, J. Q.; Jia, Y.; Li, Z.; Fan, L. L.; Cao, A. Y.; Zhu, H. W.; Wu, D. H. *Acta Mater.* **2011**, *59*, 4798.
(8) Ulbricht, M. *Polymer* **2006**, *47*, 2217.
(9) Deitzel, J. M.; Kleinmeyer, J.; Harris, D.; Tan, N. C. B. *Polymer* **2001**, *42*, 261.
(10) Huang, Z. M.; Zhang, Y. Z.; Kotaki, M.; Ramakrishna, S. *Compos. Sci. Technol.* **2003**, *63*, 2223.
(11) Reneker, D. H.; Chun, I. *Nanotechnology* **1996**, *7*, 216.
(12) Reneker, D. H.; Yarin, A. L. *Polymer* **2008**, *49*, 2387.
(13) Samuels, Y.; Wang, Z. H.; Bardelli, A.; Silliman, N.; Ptak, J.; Szabo, S.; Yan, H.; Gazdar, A.; Powell, D. M.; Riggins, G. J.; Willson, J. K. V.; Markowitz, S.; Kinzler, K. W.; Vogelstein, B.; Velculescu, V. E. *Science* **2004**, *304*, 554.
(14) Berghmans, H.; De Cooman, R.; De Rudder, J.; Koningsveld, R. *Polymer* **1998**, *39*, 4621.
(15) Lu, P.; Xia, Y. N. *Langmuir* **2013**, *29*, 7070.
(16) McCann, J. T.; Marquez, M.; Xia, Y. N. *J. Am. Chem. Soc.* **2006**, *128*, 1436.
(17) Megelski, S.; Stephens, J. S.; Chase, D. B.; Rabolt, J. F. *Macromolecules* **2002**, *35*, 8456.
(18) vandeWitte, P.; Dijkstra, P. J.; vandenBerg, J. W. A.; Feijen, J. *J. Membr. Sci.* **1996**, *117*, 1.
(19) Bognitzki, M.; Frese, T.; Steinhart, M.; Greiner, A.; Wendorff, J. H.; Schaper, A.; Hellwig, M. *Polym. Eng. Sci.* **2001**, *41*, 982.
(20) Riddick, J. A.; Bunger, W. B.; Sakano, T.; Weissberger, A. *Organic solvents: physical properties and methods of purification*; 4th ed.; Wiley Interscience: New York, 1986.
(21) Sato, S.; Gondo, D.; Wada, T.; Kanehashi, S.; Nagai, K. *Journal of Applied Polymer Science* **2013**, *129*, 1607.
(22) Horsley, L. H. *Anal. Chem.* **1947**, *19*, 508.
(23) Aitken, J. *Nature* **1913**, *90*, 619.
(24) Burkhardt, J.; Hunsche, M. *Front. Plant Sci.* **2013**, *4*, 9.
(25) Srinivasarao, M.; Collings, D.; Philips, A.; Patel, S. *Science* **2001**, *292*, 79.
(26) Briscoe, B. J.; Galvin, K. P. *J. Phys. D-Appl. Phys.* **1990**, *23*, 1265.
(27) Kumar, A.; Whitesides, G. M. *Science* **1994**, *263*, 60.
(28) Koombhongse, S.; Liu, W. X.; Reneker, D. H. *J. Polym. Sci. Pt. B-Polym. Phys.* **2001**, *39*, 2598.
(29) Casper, C. L.; Stephens, J. S.; Tassi, N. G.; Chase, D. B.; Rabolt, J. F. *Macromolecules* **2004**, *37*, 573.
(30) Yang, F.; Xu, C. Y.; Kotaki, M.; Wang, S.; Ramakrishna, S. *J. Biomater. Sci.-Polym. Ed.* **2004**, *15*, 1483.
(31) Nayani, K.; Katepalli, H.; Sharma, C. S.; Sharma, A.; Patil, S.; Venkataraghavan, R. *Ind. Eng. Chem. Res.* **2012**, *51*, 1761.
(32) Touny, A. H.; Bhaduri, S. B. *Mater. Sci. Eng. C-Mater. Biol. Appl.* **2010**, *30*, 1304.